Int. J. Electrochem. Sci., 13 **(2018)** 2118 – 2125, doi: 10.20964/2018.02.75

International Journal of
ELECTROCHEMICAL
SCIENCE
www.electrochemsci.org

Short Communication

Hydrothermal Synthesis and Electrochemical Properties of TiO_2 Nanotubes as an Anode Material for Lithium Ion Batteries

Huaimin Chen[1], *Da Chen*[2,*], *Liqun Bai*[3,*], *Kangying Shu*[2]

[1] School of Mechanical and Energy Engineering, Jimei Univeristy, Xiamen, Fujian 361021, China
[2] College of Materials Science and Engineering, China Jiliang University, Hangzhou, Zhejiang310018, China
[3] Zhejiang Provincial Key Laboratory of Chemical Utilization of Forestry Biomass, Zhejiang A & F University, Lin'an, Zhejiang Province, 311300, China
[*]E-mail: dchen_80@hotmail.com, bailiqun78@163.com

Received: 28 October 2017 / *Accepted:* 19 December 2017 / *Published:* 28 December 2017

In this work, TiO_2 nanotubes were successfully prepared by using TiO_2 nanoparticles as the precursor through a simple hydrothermal method followed by calcination. The phase structure and surface morphologies of as-prepared TiO_2 nanotubes were identified by X-ray diffraction (XRD), field-emission scanning electron microscope (FESEM) and transmission electron microscope (TEM) measurements. The as-prepared TiO_2 nanotubes presented an obvious one-dimensional nanotube structure with a tube diameter of 4~8 nm and a length of 2~10 μm. The as-prepared TiO_2 nanotubes anode delivered an initial discharge capacity of 300 mAh g^{-1} at 0.3 C, and retained a discharge capacity of 162 mAh g^{-1} (about 54% of the intial discharge capacity) after 100 cycles. The electrochemical measurements demonstrated that the as-prepared TiO_2 nanotubes anode offered a relatively high reversible capacities and good cycling stabilities, which could be attributed to the large surface area of nanotubular structure as well as the 1D nanostructure-induced fast migration of lithium ions within TiO_2 nanotubes.

Keywords: TiO_2 nanotubes; Hydrothermal synthesis; Anode materials; Lithium ion batteries

1. INTRODUCTION

In the past decades, the technology of lithium ion batteries (LIBs) has been developing very rapidly, and much progress has been already made. In the commercial LIBs, the commonly-used anodes are carbon materials (e.g., graphite). However, there are still safety concerns with carbon anode materials. Therefore, many safety alternatives have been developed to replace graphite, such as TiO_2 [1], SnO_2 [2], V_2O_5 [3], MoO_2 [4], etc. In particular, TiO_2 nanostructures as anode materials of LIBs

have gained much attention because of their superior properties [5, 6] including a relatively high capacity, a low self-discharge rate, high lithium insertion potential to avoid the formation of lithium dendrite, chemical stability, environmental benign, low cost, and the ability to be prepared with different morphologies. Compared to other nanostructures, nanotubular TiO_2 has some substantial advantages. For example, both electron and Li-ion transport path in TiO_2 nanotubes are directional and much shorter, which would benefit the electrochemical process [7]. Meanwhile, the inner and outer surface of tubular structure can provide higher electrode-electrolyte contact area, which can facilitate higher capacity and rate capability. Furthermore, the void tubular structure would also accommodate the volume expansion during the lithium ion intercalation/deintercalation process and hence achieve better electrochemical performance. Therefore, these features make nanotubular TiO_2 attractive for use as a LIB anode material, as verified by previous reports [8-12]. Wang et al. [9] reported that TiO_2 nanotubes could be prepared by using the anodic aluminum oxide (AAO) and P123 as the hard and soft template, and showed exceptional anodic electrochemical performance. Bae et al. [10] synthesized amorphous TiO_2 nanotubes through the template-directed atomic layer deposition, and demonstrated the significantly improved anodic electrochemical properties in LIBs. Recently, Panda et al. [11] investigated the influence of the tube wall thickness on the anodic electrochemical performance of TiO_2 nanotubes, which were prepared by atomic layer deposition using AAO membranes as the template. However, most of TiO_2 nanotubes were prepared by employing the hard or soft-template (such as AAO or polymer molecules) through a complex process. Thus, it is still a challenge to find a simple, inexpensive and scalable approach for the fabrication of TiO_2 nanotubes.

In the present work, TiO_2 nanotubes were prepared by a facile alkaline hydrothermal method, where commercial TiO_2 nanoparticles were used as starting materials, followed by annealing at 350 ^oC. As a LIB anode active material, the obtained TiO_2 nanotubes were then characterized by morphological and crystalline structure analysis as well as electrochemical investigation. It was found that the prepared TiO_2 nanotubes showed good electrochemical charge/discharge behavior.

2. EXPERIMENTAL

2.1 Preparation of TiO_2 nanotubes

The starting TiO_2 nanoparticles used in this study were anatase powders (titanium(IV) oxide, 20~30 nm, J&K Scientific) as supplied. TiO_2 nanotubes were synthesized by a facile alkaline hydrothermal method followed by annealing at 350 ^oC. In a typical process, 4 g of TiO_2 nanoparticles and 60 mL of glycerol were in sequence added to 60 mL of 10 M NaOH aqueous solution, followed by stirring for 2 h. The obtained dispersion solution was then transferred to a Teflon-sealed autoclave for hydrothermal reaction at 180 ^oC for 18 h. After the reaction, the products were washed using a 0.1 M HCl aqueous solution until pH = 7 to obtain the layered hydrogen titanates. The titanates were subsequently dried for 24 h at 80 ^oC, and annealed in air at 350 ^oC for 4 h to yield nanotubular TiO_2.

2.2 Materials characterizations

The morphologies of the samples were characterized by using the field emission scanning electron microscope (FESEM, JEOL JSM-6700F, Japan) and a JEOL JEM-2100 transmission electron microscope (TEM). The crystal phase identification of samples was performed on a X-ray diffraction (XRD) (Braker Axs D2 PHASER, Germany) with Cu K_α radiation (λ = 0.15406 nm). The 2θ range used in the measurements was from 5° to 80° at room temperature. The Fourier transform infrared (FTIR) absorption spectra of the samples were obtained by FTIR spectrophotometer (Bruker Tensor 27, Germany).

2.3 Electrochemical measurements

Electrochemical properties of the products were measured using coin cells. The working electrodes were prepared by casting the slurry consisting of 80 wt% of active material (the prepared TiO_2 nanotubes), 10 wt% of conductive Super P carbon black as conductive additive, and 10 wt% of poly (vinylidene fluoride) (PVDF) (Alfa Aesar) as binding agent onto a copper foil. The electrolyte consisted of a solution of 1 M $LiPF_6$ in ethylene carbonate (EC)/diethylcarbonate (DEC) (1 : 1, v/v). Lithium foil was used as counter electrodes. These cells were assembled in an argon-filled glovebox (Super 1220/750, MIKROUNA) and galvanostatically cycled between 1.0 and 3.0 V (vs. Li/Li^+) on a multi-channel battery cycler (Land Battery Test System).

3. RESULTS AND DISCUSSION

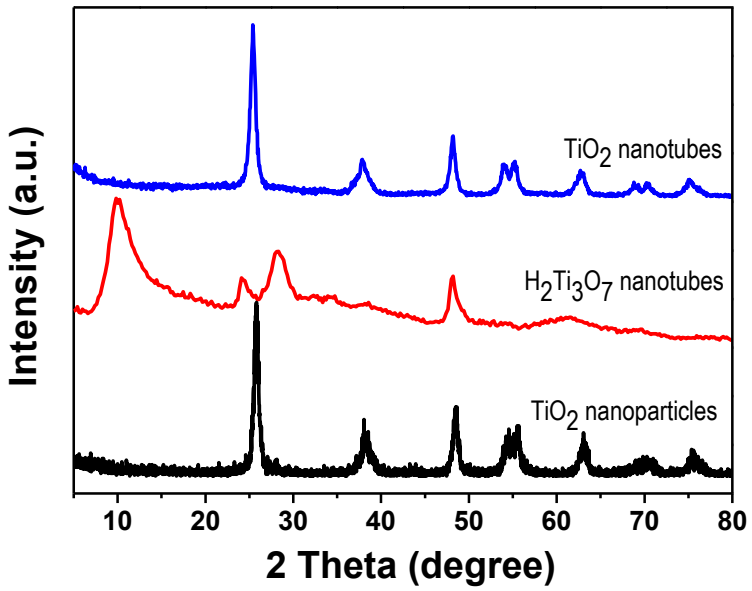

Figure 1. XRD patterns of (a) the precursor of commercial TiO_2 nanoparticles, (b) the prepared intermediate of $H_2Ti_3O_7$ nanotubes, and (c) the prepared product of TiO_2 nanotubes.

Figure 1 shows the XRD patterns of the starting material (TiO_2 nanoparticles), the intermediate product ($H_2Ti_3O_7$ nanotubes) and the final product (TiO_2 nanotubes). For the TiO_2 nanoparticles, all diffraction peaks could be well indexed as phase-pure anatase TiO_2. After the hydrothermal treatment of the TiO_2 nanoparticles, no TiO_2 diffraction peaks were observed, and new diffraction peaks corresponding to the monoclinic phase of $H_2Ti_3O_7$ (JCPDS no. 36-0654) were observed. After annealing at 350 ^oC, however, the monoclinic phase of $H_2Ti_3O_7$ disappeared and anatase TiO_2 phase reappeared, suggesting that the monoclinic phase of $H_2Ti_3O_7$ after calcination could be transformed into anatase TiO_2. The XRD result confirmed the successful preparation of anatase TiO_2 nanotubes.

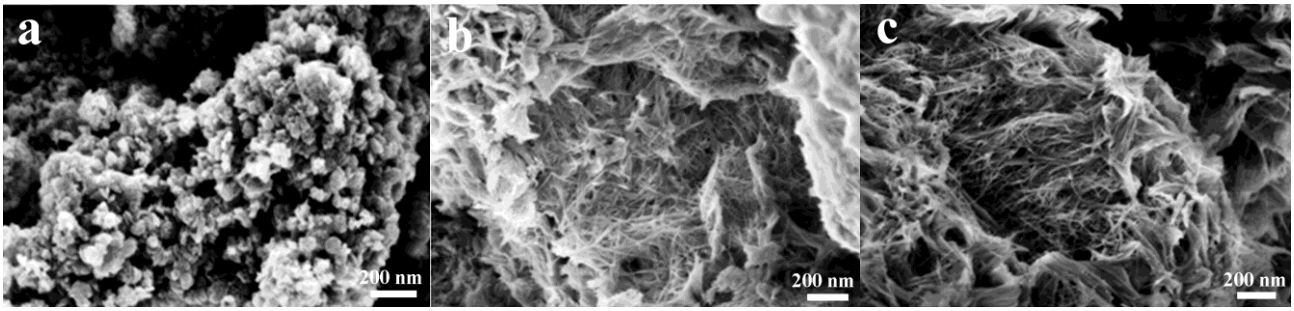

Figure 2. FESEM images of (a) the precursor of commercial TiO_2 nanoparticles, (b) the prepared intermediate of $H_2Ti_3O_7$ nanotubes, and (c) the prepared product of TiO_2 nanotubes.

Figure 2 shows the FESEM images of the starting material (TiO_2 nanoparticles), the intermediate product ($H_2Ti_3O_7$ nanotubes), and the final product (TiO_2 nanotubes). As shown, the TiO_2 nanoparticles (Figure 2a) had a morphology of granular structure, and were prone to aggregate. After the hydrothermal process, however, the obtained intermediate product (Figure 2b) exhibited an obvious one-dimensional nanotube structure with a tube diameter of 4~8 nm and a length of 2~10 μm. When the intermediate product ($H_2Ti_3O_7$) was transferred to TiO_2 after annealing, the final product could also preserve the tubular structure (Figure 2c). To further reveal the morphological features of the starting material, intermediate and final product, we performed the TEM measurements, as shown in Figure 3. The TiO_2 nanoparticles (Figure 3a) were uniform in shape with a particle size of ca. 10 nm, but exhibited a serious aggregation. The TEM image of the intermediate product (Figure 3b) clearly reveals a relatively uniform nanotubular structure with a diameter of 4~8 nm, indicating the morphological evolution from granular to nanotubular structure induced by the hydrothermal treatment. After calcination at 350 ^oC, the tubular structure was well preserved, and the TiO_2 nanotubes were thus obtained (Figure 3c). This means that the calcination process would not destroy the tubular structure of the $H_2Ti_3O_7$ intermediate, but would dehydrate the $H_2Ti_3O_7$ nanotubes to form TiO_2 nanotubes.

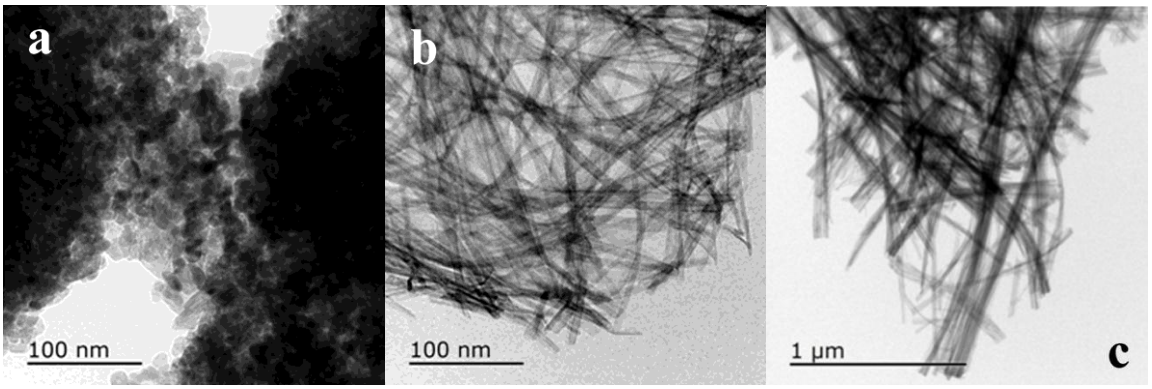

Figure 3. TEM images of (a) the precursor of commercial TiO_2 nanoparticles, (b) the prepared intermediate of $H_2Ti_3O_7$ nanotubes, and (c) the prepared product of TiO_2 nanotubes.

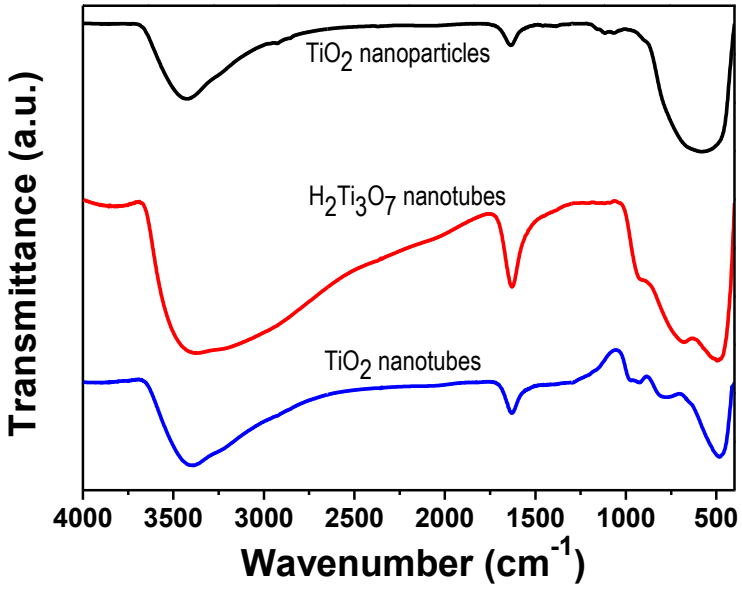

Figure 4. FT-IR spectra of (a) the precursor of commercial TiO_2 nanoparticles, (b) the prepared intermediate of $H_2Ti_3O_7$ nanotubes, and (c) the prepared product of TiO_2 nanotubes.

In addition, FTIR spectra were examined to uncover the surface characteristics of the samples. Figure 4 displays the FT-IR spectra of starting materials, intermediates and products. For all the three samples, the wide characteristic peaks at 3450 cm^{-1} could be assigned to the stretching vibration of surface-absorbed H_2O molecules or surface hydroxyl groups, which could be asscribed to the physically absorbed water. The absorption peak at ca. 1670 cm^{-1} was contributed to the characteristic peaks of surface O-H bonds corresponding to the bending vibration of surface hydroxyl groups. Obviously, the absorption intensities of the stretching or bending vibration of surface hydroxyl groups for the TiO_2 nanotubes sample were much weaker than those for the $H_2Ti_3O_7$ nanotubes samples, indicating that the absorbed water on the $H_2Ti_3O_7$ surface was mostly removed after annealing at 350 ^oC. In addition, there was a wide and strong absorption peak between 500 ~ 1000 cm^{-1}, which could be ascribed to the stretching or deviational vibration of Ti-O-Ti bonds of TiO_2 [5, 13]. It was found that

the peak absorption width of the Ti-O-Ti vibration mode for the TiO_2 nanotubes sample was narrowed compared to the $H_2Ti_3O_7$ nanotubes sample, suggesting that the annealing process would facilitate the bonding formation between titanium and oxygen atoms [14], thus leading to the transformation of monoclinic $H_2Ti_3O_7$ to anatase TiO_2.

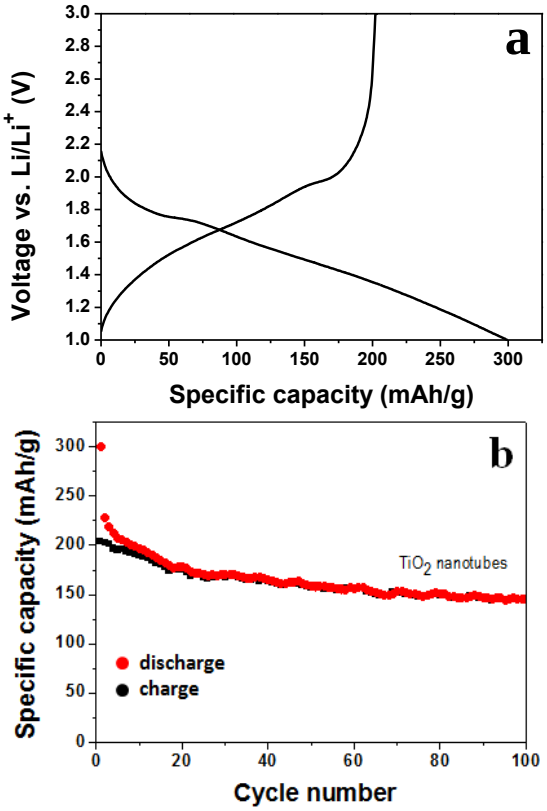

Figure 5. The first cycle charge–discharge voltage profile (a), and the discharge (red curve) and charge (black curve) cycling performance (b) of the cells with the prepared TiO_2 nanotubes anode between 1.0 and 3.0 V at 0.3 C rate.

The electrochemical performance of as-prepared TiO_2 nanotubes anode was investigated by cycling at room temperature from a coin-type half cell using Li metal as the counter electrode. Figure 5 shows the first cycle charge–discharge voltage profiles and cycling performance of the cells with the prepared TiO_2 nanotubes electrode between 1.0 and 3.0 V at 0.3 C rate. As demonstrated in Figure 5a, a charge voltage plateau at 2.05 V and a discharge plateau at 1.75 V appeared, which were associated with the lithium insertion and extraction in the anatase lattice, respectively [15]. The first discharge and charge capacities of the TiO_2 nanotubes electrode was about 300 and 204 mAh g^{-1}, respectively, with a coulombic efficiency of ~68%. The initial irreversible capacity loss was mainly attributed to the decomposition of the electrolyte and the solid/electrolyte interphase (SEI) formation on the electrode surface [16]. The capacity retention as a function of cycle number is illustrated in Figure 5b. As seen, with increasing the cycle number, the capacities of the cell was decayed rapidly at preliminary stage, and then decreased slowly at the latter stage. After 100 cycles, the discharge and charge capacities

were decreased to ca. 162 mAh g^{-1} (~54% of the initial discharge capacity) and 161.5 mAh g^{-1} (~79% of the initial charge capacity), respectively, confirming a pretty good cycling performance of the prepared TiO_2 nanotube anode which was comparable with those of previously-reported TiO_2 nanotubes in literature (Table 1). Moreover, the Coulombic efficiency was only 68% for the first cycle, and after several cycles was rapidly promoted to above 95% after several cycles, and then was pretty steady around 99%, suggesting an excellent charge-discharge efficiency. The pretty good cycling performance of the prepared TiO_2 nanotube anode could be mainly ascribed to the large surface area of nanotubular structure as well as the 1D nanostructure-induced fast migration of lithium ions within TiO_2 nanotubes [17, 18].

Table 1. Electrochemical performance of the prepared TiO_2 nanotubes in comparison with the previously-reported TiO_2 nanotubes

Sample	Preparation method	Initial discharge capacity (mAh g^{-1})	Discharge capacity after cycles (mAh g^{-1})	Reference
Mesoporous TiO_2 nanotubes	AAO membranes -templated sol-gel	303 (current density: 1 A g^{-1}; potential range: 1.2~3.0 V (vs. Li^+/Li)	162 (after 100 cycles) (current density: 1 A g^{-1}; potential range: 1.2~3.0 V (vs. Li^+/Li)	9
Hierarchical TiO_2 nanotubes	atomic layer deposition	~655 (current density: 1 C; potential range: 0.7~3.0 V (vs. Li^+/Li)	~170 (after 7 cycles) (current density: 1 C; potential range: 0.7~3.0 V (vs. Li^+/Li)	10
Arrayed TiO_2 nanotubes	alumina membrane -templated atomic layer deposition	260 (current density: 1 C; potential range: 0.7~3.0 V (vs. Li^+/Li)	250 (after 500 cycles) (current density: 1 C; potential range: 0.7~3.0 V (vs. Li^+/Li)	11
TiO_2 nanotube arrays	anodic oxidation	253 (current density: 0.1 C; potential range: 1.0~2.5 V (vs. Li^+/Li)	186 (after 30 cycles) (current density: 0.1 C; potential range: 1.0~2.5 V (vs. Li^+/Li)	12
TiO_2 nanotubes	Hydrothermal synthesis	300 (current density: 0.3 C; potential range: 1.0~3.0 V (vs. Li^+/Li)	162 (after 100 cycles) (current density: 0.3 C; potential range: 1.0~3.0 V (vs. Li^+/Li)	This work

4. CONCLUSIONS

In summary, anatase TiO_2 nanotubes were successfully prepared by using a simple hydrothermal method followed by calcination. The prepared TiO_2 nanotubes possessed a uniform tubular structure with a tube diameter of 4~8 nm and a length of 2~ 10 μm. The cells based on the prepared TiO_2 nanotubes delivered an initial discharge capacity of 300 mAh g^{-1} at 0.3 C, and maintained a discharge capacity of 162 mAh g^{-1} (54% of the first discharge capacity) after 100 cycles. This work demonstrates that the as-prepared TiO_2 nanotubes anode possessed a relatively high reversible capacities and pretty good cycling performance, indicating its great potential for use as an anode material for high-performance LIBs.

ACKNOWLEDGEMENTS
This work is financially supported by Zhejiang Provincial Natural Science Foundation of China (No. LY17E020009), CAS Key Laboratory of Design and Assembly of Functional Nanostructures, Fujian Institute of Research on the Structure of Matter, Chinese Academy of Sciences, China (No. 2013DP173231), Pre-research Project of Research Center of Biomass Resource Utilization, Zhejiang

A & F University (No. 2013SWZ02-3), and Zhejiang Provincial Key Lab. for Chem. & Bio. Processing Technology of Farm Products (No: 2016KF0002).

References

1. J. F. Ye, W. Liu, J. G. Cai, S. Chen, X. W. Zhao, H. H. Zhou and L. M. Qi, *J. Am. Chem. Soc.*, 133 (2011) 933-940.
2. J. S. Chen and X. W. Lou, *Small*, 9 (2013) 1877-1893.
3. J. Liu, H. Xia, D. F. Xue and L. Lu, *J. Am. Chem. Soc.*, 131 (2009) 12086.
4. Y. M. Sun, X. L. Hu, Jimmy C. Yu, Q. Li, W. Luo, L. X. Yuan, W. X. Zhang and Y. H. Huang, *Energy Environ. Sci.*, 4 (2011) 2870-2877.
5. B. Wang, J. Cheng and Y. Wu, *J. Alloy Compd.*, 527 (2012) 132-136.
6. D. V. Bavykin, J. M. Friedrich and F. C. Walsh, *Adv. Mater.*, 18 (2006) 2807-2824.
7. J. Li, W. Wan, F. Zhu, Q. Li, H. Zhou, J. Li and D. Xu, *Chem. Commun.*, 48 (2012) 389-391.
8. Q. W. Wang, X. F. Du, X. Z. Chen and Y. L. Xu, *Acta Phys.-Chim. Sin.*, 31 (2015) 1437-1451.
9. K. Wang, M. Wei, M. A. Morris, H. Zhou and J. D. Holme, *Adv. Mater.*, 19 (2007) 3016-3020.
10. C. Bae, Y. Yoon, W. S. Yoon, J. Moon, J. Kim and H. Shin, *ACS Appl. Mater. Interfaces*, 2 (2010) 1581-1587.
11. S. K. Panda, Y. Yoon, H. S. Jung, W. S. Yoon and H. Shin, *J. Power Sources*, 204 (2012) 162-167.
12. T. Anwar, L. Wang, T. X. Liang, X. M. He, R. U. R. Sagar and K. Shehzad, *Int. J. Electrochem. Sci.*, 10 (2015) 6537-6547.
13. B. B. Ni, F. Li, X. N. Li, Z. P. Fu, Y. W. Zhu and Y. L. Lu, *Appl. Surf. Sci.*, 283 (2013) 175-180.
14. H. Yin, Y. Wada, T. Kitamura, S. Kambe, S. Murasawa, H. Mori, T. Sakata and S. Yanagida, *J. Mater. Chem.*, 11 (2001) 1694-1703.
15. H. Lindström, S. Södergren, A. Solbrand, H. Rensmo, J. Hjelm, A. Hagfeldt and S. E. Lindquist, *J. Phys. Chem. B*, 101 (1997) 7717-7722.
16. A. Pozio, M. Carewska, F. Mura, R. D'Amato, M. Falconieri, M. De Francesco and G. B. Appetecchi, *J. Power Sources*, 247 (2014) 883-889.
17. W. J. Macklin and R. J. Neat, *Solid State Ion*s, 53-56 (1992) 694-700.
18. R. van de Krol, A. Goossens and J. Schoonman, *J. Phys. Chem. B*, 103 (1999) 7151-7159.